International Journal of Nanomedicine

Dovepress
Taylor & Francis Group

Open Access Full Text Article

ORIGINAL RESEARCH

MoS_{2-x}/C Nanosheets for Antifungal and Anti-Inflammatory Therapy of *Aspergillus fumigatus* Keratitis in Mice

Zhuhui Feng[1], Jing Lin[1], Qian Wang[1], Lina Zhang[1], Lingwen Gu[1], Bing Yu[1], Xueyun Fu[1], Daohao Li[2], Guiqiu Zhao[1], Cui Li[1]

[1]Department of Ophthalmology, The Affiliated Hospital of Qingdao University, Qingdao, Shandong, People's Republic of China; [2]State Key Laboratory of Bio-Fibers and Eco-Textiles, School of Environmental Science and Engineering, College of Materials Science and Engineering, Qingdao University, Qingdao, Shandong, People's Republic of China

Correspondence: Guiqiu Zhao; Cui Li, Department of Ophthalmology, Affiliated Hospital of Qingdao University, 16 Jiangsu Road, Qingdao, Shandong, 266003, People's Republic of China, Email zhaoguiqiu_good@126.com; yankelicui@126.com

Purpose: To investigate the therapeutic potential of sulfur vacancy-molybdenum disulfide/carbon composite nanosheets (MoS_{2-x}/C NS) in *Aspergillus fumigatus (A. fumigatus)* keratitis in mice.

Methods: The in vitro antifungal efficacy of MoS_{2-x}/C NS against *A. fumigatus* was evaluated by propidium iodide (PI) staining, minimum inhibitory concentration (MIC) determination, and biofilm formation assays. Toxicity assessments of the MoS_{2-x}/C NS were conducted using a Lactate dehydrogenase (LDH) assay kit for in vitro cytotoxicity and the Draize eye test for in vivo ocular irritation. The severity of fungal keratitis in mice was assessed using clinical scoring, plate counting, and hematoxylin and eosin (H&E) staining. The anti-inflammatory efficacy of MoS_{2-x}/C NS was determined by quantifying inflammatory factor levels using reverse transcription polymerase chain reaction (RT-PCR).

Results: In vitro, MoS_{2-x}/C NS significantly inhibited *A. fumigatus* growth, demonstrated favorable biocompatibility, and reduced the expression of IL-6 and TNF-α in human corneal epithelial cells (HCECs) stimulated by inactivated *A. fumigatus* hyphae. In vivo, MoS_{2-x}/C NS treatment significantly reduced fungal load, attenuated pathological corneal damage, and suppressed IL-6 and TNF-α levels, effectively alleviating *A. fumigatus* keratitis in mice.

Conclusion: This study demonstrates that MoS_{2-x}/C NS possesses significant therapeutic potential for fungal keratitis mediated through dual antifungal and anti-inflammatory mechanisms, thereby improving the prognosis of *A. fumigatus* keratitis.

Keywords: MoS_{2-x}/C NS, sulfur vacancy, *Aspergillus fumigatus* keratitis, antifungal, anti-inflammatory, nanomaterial therapy

Introduction

Fungal keratitis, a sight-threatening ocular infection, exhibits a high global incidence, accounting for 6-53% of infectious keratitis cases with >1 million annual occurrences in developing countries.[1–3] The primary predisposing factors include corneal injury, prolonged contact lens wear and a medical history of systemic conditions.[4] Current antifungal therapies demonstrate limited efficacy due to ocular surface physiological barriers, poor corneal drug permeability, and emerging fungal resistance.[5] Recently, novel antimicrobial technologies utilizing innovative nanomaterial have emerged, offering new therapeutic avenues for fungal keratitis treatment and demonstrating potential in addressing drug resistance.[6–8]

Molybdenum disulfide (MoS_2), a transition metal dichalcogenide, has been extensively studied due to its exceptional optical, electronic, chemical, and mechanical properties. Its substantial specific surface area and ease of functionalization have garnered significant attention in biomedical applications, positioning MoS_2 as a promising nanomaterial for antimicrobial agents, biosensors, and drug delivery systems.[9–12] In particular, MoS_2-based nanomaterials offer a promising strategy for treating infected wounds.[13,14] Recent studies further demonstrate that MoS_2 exhibit antibacterial activity against both Gram-positive *Staphylococcus aureus* and methicillin-resistant *Staphylococcus aureus (MRSA)*.[15,16]

Received: 27 July 2025
Accepted: 29 October 2025
Published: 10 December 2025

Nevertheless, research on the antifungal properties of MoS_2 with sulfur-vacancy remains limited. Currently, only a few studies suggest the potential of MoS_2 in addressing fungal pathogens related to agricultural production and environmental pollution.[17–21] These findings indicated that MoS_2 nanoparticles could effectively inhibit the growth of *Fusarium graminearum* and *Saccharomyces uvarum* by inducing oxidative stress and cellular damage. Furthermore, this antifungal effect was enhanced by sulfur vacancies. Building on this evidence, we hypothesize that sulfur-vacancy-engineered MoS_2 also acts against fungal keratitis by disrupting fungal morphology and growth.

It is well-established that fungi can breach the damaged corneal epithelial barrier and invade the deeper tissues of the cornea, thereby activating local immune responses to facilitate fungal clearance.[22] However, an excessive inflammatory response secondary to fungal infection can result in further damage to corneal tissue.[23–25] Researches have highlighted that controlling this excessive inflammatory response is essential for improving the prognosis of fungal keratitis.[26–28] Notably, MoS_2 has demonstrated significant anti-inflammatory properties in models of neurological inflammation and osteoarthritis,[29,30] yet its potential in treating ocular infections remains unexplored. Based on these findings, we further hypothesize that MoS_2 may also exert anti-inflammatory effects in the context of fungal keratitis.

In this study, we synthesized MoS_{2-x}/C NS and evaluated its dual antifungal and anti-inflammatory properties. In vitro, the material demonstrated biocompatibility and inhibited TNF-α, IL-6, and reactive oxygen species (ROS) production in response to fungal hyphae, while also potently suppressing *A. fumigatus* spore germination, biofilm formation, and disrupting its cell membrane. In mice model of fungal keratitis, MoS_{2-x}/C NS treatment markedly attenuated the infection, reducing fungal burden, corneal edema, inflammatory infiltration, and cytokine levels. The observed promotion of corneal epithelial cell migration further indicates its capacity to support healing. These findings demonstrate that MoS_{2-x}/C NS represents a promising therapeutic strategy for fungal keratitis.

Materials and Methods

Materials

Ammonium molybdate tetrahydrate ($(NH_4)_6Mo_7O_{24}\cdot 4H_2O$), thiourea ($H_2NCSNH_2$), hydrazine hydrate solution ($H_4N_2\cdot H_2O$) and acetic acid were obtained from Sinopharm Chemical Reagent Co., Ltd. (Shanghai, China). Sodium alginate (SA) was acquired from Aladdin Reagent Co., Ltd. (Shanghai, China).

Animal Experiments

Female 8-week-old C57BL/6 mice were purchased from Huachuangxinnuo Co., Ltd. (Jiangsu, China). The animal experiments complied with the National Research Council's Guide for the Care and Use of Laboratory Animals and were approved by the Ethics Committee of the Affiliated Hospital of Qingdao University (QYFYWZLL 29840).

Preparation of MoS_{2-x}/C Composite Nanomaterial

The preparation schematic is illustrated in Scheme 1. Initially, ammonium molybdate tetrahydrate (0.124 g) and thiourea (0.22 g) were dissolved into 20 mL pure water. Concurrently, 0.3 mL of acetic acid and SA (0.15 g) were added to 30 mL pure water and mixed thoroughly. Subsequently, the two solutions were combined in a reaction kettle for a hydrothermal reaction at 180°C for 24 hours. Upon completion of the hydrothermal reaction, the mixture was cooled to room temperature (RT). The sample was then rinsed repeatedly with deionized water and ethanol, followed by drying in an oven at 70°C for 12 hours. After drying, the sample was naturally cooled to RT and carbonized at 800°C for 2 hours to yield the MoS_2/C composite material. Finally, 3 mL of hydrazine hydrate solution was added to 100 mg of the MoS_2/C composite material, and the mixture was reacted for 3 hours to produce the MoS_{2-x}/C composite material with sulfur vacancies.[31]

Characterization of MoS_{2-x}/C Composite Nanomaterial

The microstructures and morphology of the sample were investigated using transmission electron microscopy (TEM), scanning electron microscopy (SEM), high angle annular dark field scanning transmission electron microscopy (HAADF-STEM) and atomic force microscopy (AFM). The distribution of molybdenum (Mo), sulfur (S), and carbon

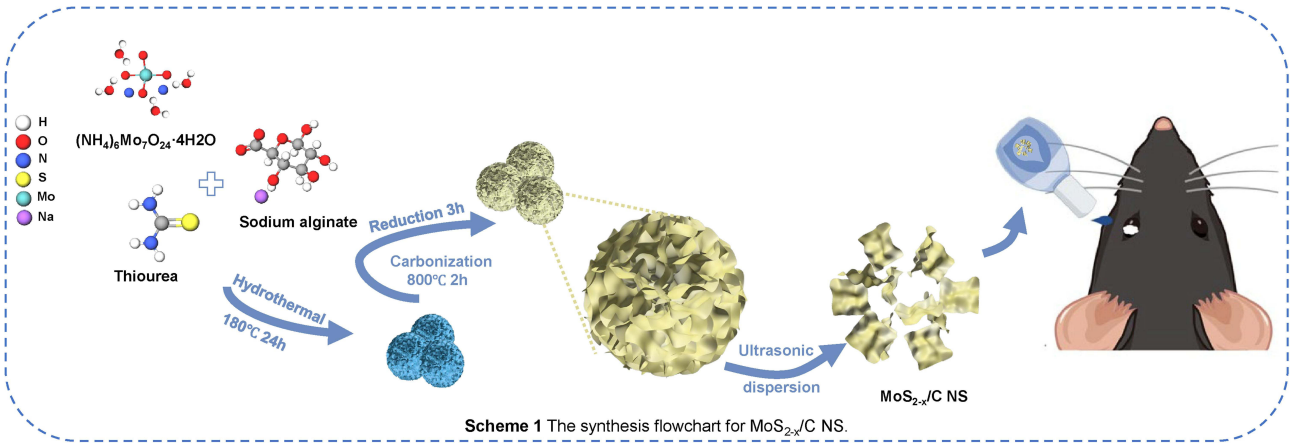

Scheme 1 The synthesis flowchart for MoS_{2-x}/C NS.

(C) elements on the material surface was analyzed through X-ray energy dispersive spectroscopy (EDS) mapping. Additionally, the prepared materials were characterized and analyzed using electron paramagnetic resonance (EPR), X-ray diffraction (XRD), X-ray photoelectron spectroscopy (XPS) and Raman spectroscopy.

Lactate Dehydrogenase (LDH) Assay of Cells

The cytotoxicity of MoS_2/C NS or MoS_{2-x}/C NS to human corneal epithelial cells (HCECs) was assessed using the LDH assay. The LDH assay is a standard method for quantifying cell death, based on the measurement of LDH released from damaged cell membranes.[32] Replace the culture medium containing HCECs with varying concentrations (0, 20, 40, 80, 160, and 320 μg/mL) of MoS_2/C NS or MoS_{2-x}/C NS. After co-culturing for 24 hours, utilize an LDH detection kit (Beyotime Biotechnology, Jiangsu, China) to assess the cytotoxic effects of MoS_2/C and MoS_{2-x}/C NS on HCECs by measuring the total intracellular LDH content. The experimental procedures were conducted according to the instructions provided by the reagent kit. After incubation at RT in the dark for 30 minutes, the optical density was detected at 490 nm and 600 nm, respectively.

Mice's Draize Eye Test

To evaluate the impact of MoS_{2-x}/C NS on the normal corneal epithelium in vivo, the Draize eye test was performed in mice to quantitatively assess the severity of any adverse effects.[33] Healthy female C57BL/6 mice, aged eight months and exhibiting normal anterior segments, were immediately divided into two groups. The treatment complied with the ARVO Statement for the Use of Animals on Ophthalmic and Vision Research. In experimental group, 4 μL of MoS_{2-x}/C NS (160 μg/mL) dispersion was administered to left conjunctival sac, while the control group received 4 μL of PBS solution in the same manner, four times daily. The right corneas of both groups were left untreated. On days 1, 3, and 5 post-treatment, fluorescein sodium staining was conducted on the mouse corneas using an ophthalmic slit lamp, with cobalt blue light employed to assess surface irritation of the mouse eyes. The results were recorded and evaluated according to the standards.[34]

The Cell Scratching Test of HCECs

The cell scratch assay was performed to assess the effect of MoS_{2-x}/C NS on the migratory ability of HCECs in vitro. Before inoculating HCECs, the bottom of each well was marked with three parallel lines in a 6-well plate using a black marker. The incubated 6-well plate was then placed in a cell culture incubator. The HCECs were cultivated until confluence reached 70% to 80%. Following this, serum-free Dulbecco's Modified Eagle's Medium (DMEM) cell culture medium was replaced and incubated overnight. To be specific, a 200 μL pipette tip was employed to draw three perpendicular lines across the black marker lines in each well, and the wells were washed with sterile PBS. Serum-free DMEM cell culture medium containing varying concentrations of MoS_{2-x}/C NS (0, 80, and 160 μg/mL) was added to

treat the HCECs. After 24 hours, the area of the scratch was measured to evaluate the migration ability of HCECs. Images were photographed using the EVOS™ M5000 imaging system.

Calcofluor White (CFW) Staining and Minimum Inhibitory Concentration (MIC) of *A. fumigatus*

To evaluate the antifungal activity of MoS_2/C NS or MoS_{2-x}/C NS against *A. fumigatus*, we employed CFW staining and MIC assays.[35] A spore suspension (1×10^5 CFU/mL) was prepared, to which MoS_2/C or MoS_{2-x}/C NS were added separately. The final concentrations of the materials were adjusted to 20, 40, 80, 160, and 320 μg/mL. The mixture was thoroughly mixed and subsequently added to a 96-well plate. Initial absorbance was determined at 540 nm. The culture plate was then incubated for 24 hours, after which the absorbance was re-evaluated at the same wavelength. Then the mycelium was gently washed with sterile PBS, and 50 μL CFW staining solution was joined to each well. Images were pictured using a fluorescence inverted microscope after a 15-minute incubation in the dark.

Biofilm Formation and Inhibition Test

The antifungal effect was further evaluated using a biofilm formation and inhibition assay.[36] MoS_{2-x}/C NS was added to a spore suspension (1×10^5 CFU/mL), resulting in final material concentrations of 5, 10, 20, 40, 80, and 160 μg/mL. After co-culturing for 24 hours in a 24-well plate, the culture medium was discarded, and sterile PBS was used to rinse each well gently. Subsequently, the culture plate was dried at RT. The biofilm was then fixed using a glutaraldehyde solution for 20 minutes. Subsequently, 0.1% crystal violet solution was joined and allowed to stain for 15 minutes. Each well was then washed gently and repeatedly with PBS until the rinsing solution showed no discernible color. Afterward, 200 μL of 95% ethanol solution was added for decolorization. Finally, the ethanol solution was transferred to a new 96-well plate, and absorbance was observed at 570 nm.

Propidium Iodide (PI) Staining

PI staining was used to assess the integrity of the fungal cell membrane.[37] A spore suspension of *A. fumigatus* (1×10^5 CFU/mL) was transferred into 6-well plates. After incubated for 24 hours, culture medium was replaced with either 160 μg/mL MoS_2/C NS or MoS_{2-x}/C NS. The plates were incubated in constant temperature incubator for an additional 24 hours. Subsequently, culture medium was discarded. Mycelium was gently washed with sterile PBS before PI staining solution was added. The plates were then incubated for 15 minutes in the dark, after which images were pictured and recorded using fluorescence inverted microscope.

Mice Fungal Keratitis Models

Healthy eight-month-old female C57BL/6 mice with normal anterior segments were general anesthetized. Subsequently, a deep tunnel was created within the corneal stroma at the pupillary margin on a microscope operating table. The spore suspension of *A. fumigatus* (1×10^7 CFU/mL) was injected using a microinjector to establish a model of *A. fumigatus* keratitis through the tunnel. The degree of corneal opacity in the mice was observed daily with a slit lamp, and local eye drops were administered four times a day. The experimental group received 160 μg/mL MoS_{2-x}/C NS dispersion in the left eye, while the control group was handled with a PBS solution in the left eye. The right eyes of both groups remained untreated. Observations of corneal infection were conducted using an ophthalmic slit lamp. At 1, 3 and 5 days post-infection (p.i.), clinical scoring along with photographic documentation was performed according to the standards.[38]

Plate Count

The fungal load in the cornea was determined by the plate counting.[39] On the 3 days p.i., corneas of mice were harvested and thoroughly homogenized to produce a corneal homogenate. This homogenate was then uniformly incubated onto a solid Sabouraud culture dish. The culture dish was incubated for observation. Once surface colonies formed, photographs were taken, and the number of colonies on the surface was recorded.

Table 1 Primer Sequences

Gene	Primer Sequence (5'-3')	Gene Bank
β-actin (mouse)	F: GATTACTGCTCTGGCTCCTAGC R: GACTCATCGTACTCCTGCTTGC	NM_007393.5
TNF-α (mouse)	F: ACCCTCACACTCAGATCATCTT R: GGTTGTCTTTGAGATCCATGC	NM_013693.3
IL-6 (mouse)	F: TGATGGATGCTACCAAACTGGA R: TGTGACTCCAGCTTATCTCTTGG	NM_001314054.1
GAPDH (human)	F: TGGCACCCAGCACAATGAA R: CTAAGTCATAGTCCGCCTAGAAGCA	NM_001101.5
IL-6 (human)	F: AAGCCAGAGCTGTGCAGATGAGTA R: TGTCCTGCAGCCACTGGTTC	NM_000600.5
TNF-α (human)	F: TGCTTGTTCCTCAGCCTCTT R: CAGAGGGCTGATTAGAGAGAGGT	NM_000594.4

Inactivated *A. fumigatus* Stimulation

HCECs were cultured until they reached 80% confluence. The culture medium was replaced and added inactivated *A. fumigatus* mycelium to each well to stimulate the cells for 2 hours. Subsequently, MoS_{2-x}/C NS was added to corresponding wells, and the cells were co-cultured for an additional 6 hours.

Reverse transcription polymerase chain reaction (RT-PCR)

At 3 days p.i., corneas of mice were collected. Total RNA from HCECs and corneas was isolated using RNAiso Plus reagent. Then, reverse transcription was used to synthesize complementary DNA. RT-PCR was conducted following the protocols established in a prior experiment.[40] The primer sequences of our experiment are detailed in Table 1.

ROS Assay

The ROS assay was utilized to evaluate the ROS-scavenging ability of MoS_{2-x}/C NS.[41] HCECs were incubated into a 6-well plate for 24 hours. Once a cell fusion degree of 80% was reached, the cells were pre-stimulated with inactivated *A. fumigatus* hyphae. After one hour of stimulation, the cells were treated with MoS_{2-x}/C NS. After 24 hours of stimulation with inactivated *A. fumigatus* hyphae, H_2O_2 reagent was used to the normal positive control group. Experimental steps were according to the instructions of the ROS detection kit (Beyotime Biotechnology, Jiangsu, China). The negative control group received no treatment. Subsequently, the serum-free medium containing 10 μM DCFH-DA was replaced, and the plate was incubated for 30 minutes in the dark. After incubation, each well was washed with serum-free culture medium. Finally, images were pictured using the EVOS™ M5000 imaging system.

Statistical Analysis

GraphPad 9.0 software was performed to the analysis of the data. The data were presented as mean ± SD. One-way ANOVA was utilized for comparisons involving three or more groups. A two-tailed Student's *t*-test was adopted to compare experimental data between two groups. Differences in clinical scores and CFS scores between the PBS and MoS_{2-x}/C NS-treated groups were analyzed using two-way ANOVA. A *P*-value of less than 0.05 indicates that the difference is statistically significant. Each experiment was independently conducted three times.

Results and Discussion

Preparation and Characterization of MoS_{2-x}/C NS

MoS_2/C composite material with sulfur vacancies was synthesized using hydrothermal and chemical reduction methods, as illustrated in Scheme 1. SA served as a carbon source, possessing numerous carboxyl groups that facilitated strong coordination with molybdenum atoms, thereby reducing the layered structure of MoS_2. Following the removal of specific sulfur atoms from MoS_2/C NS using hydrazine hydrate, MoS_{2-x}/C NS with sulfur vacancies was produced. A dispersion

 https://doi.org/10.2147/IJN.S552664

of MoS_{2-x}/C NS exhibiting good dispersibility was prepared through ultrasonic dispersion. SEM image (Figure 1A) revealed that MoS_{2-x}/C NS possessed layered, stacked spherical structures. TEM (Figure 1B) image illustrated that the stacked spherical structures were composed of ultra-thin layers. HAADF-STEM (Figure 1C) clearly showed the existence of sulfur vacancies on the surface of MoS_{2-x}/C NS. The AFM image (Figure 1D) indicated that the thickness of MoS_{2-x}/C NS is less than 1.9 nm, thereby confirming the structure of MoS_{2-x}/C NS. And HAADF-STEM (Figure 1E) image illustrated the layers of MoS_{2-x}/C NS were curled and folded. The EDS mapping images (Figure 1F–H) revealed that the Mo, S, and C elements were uniformly distributed across the surface of MoS_{2-x}/C NS. Additionally, the XRD spectra (Figure 1I), Raman spectra (Figure 1J), and XPS spectra (Figure 1K) exhibited characteristic peaks of MoS_2, confirming that the crystal structure of the material remained unchanged during the formation of sulfur vacancies. EPR (Figure 1L) demonstrated that, in comparison to MoS_2/C, the characteristic peak (g=1.928) associated with Mo-S dangling bonds in MoS_{2-x}/C nanomaterial was intensified, signifying the formation of sulfur vacancies. This observation indicated the successful preparation of MoS_{2-x}/C NS.

In vitro Antifungal Effect of MoS_{2-x}/C NS on *A. fumigatus*

The MIC analysis indicated that both MoS_2/C NS (Figure 2A) and MoS_{2-x}/C NS (Figure 2B) began to inhibit the sprouting of *A. fumigatus* spores at a concentration of 20 μg/mL, with the inhibitory effect being concentration-dependent. At concentrations below 320 μg/mL, the antifungal efficacy of MoS_{2-x}/C NS surpassed that of MoS_2/C NS (Figure 2C). CFW staining results demonstrated that, compared to the control group (Figure 2D), the fluorescence intensity of MoS_2/C NS (Figure 2E) and MoS_{2-x}/C NS (Figure 2F) treatment groups decreased, suggesting a reduction in the number of hyphae. The fluorescence intensity in the MoS_{2-x}/C NS treatment group was weaker than MoS_2/C NS, indicating a more pronounced inhibitory effect on hyphal growth. Additionally, PI staining results revealed that the fungal hyphae in the control group were almost unstained (Figure 2G). In contrast, the fungal hyphae in the 160 μg/mL

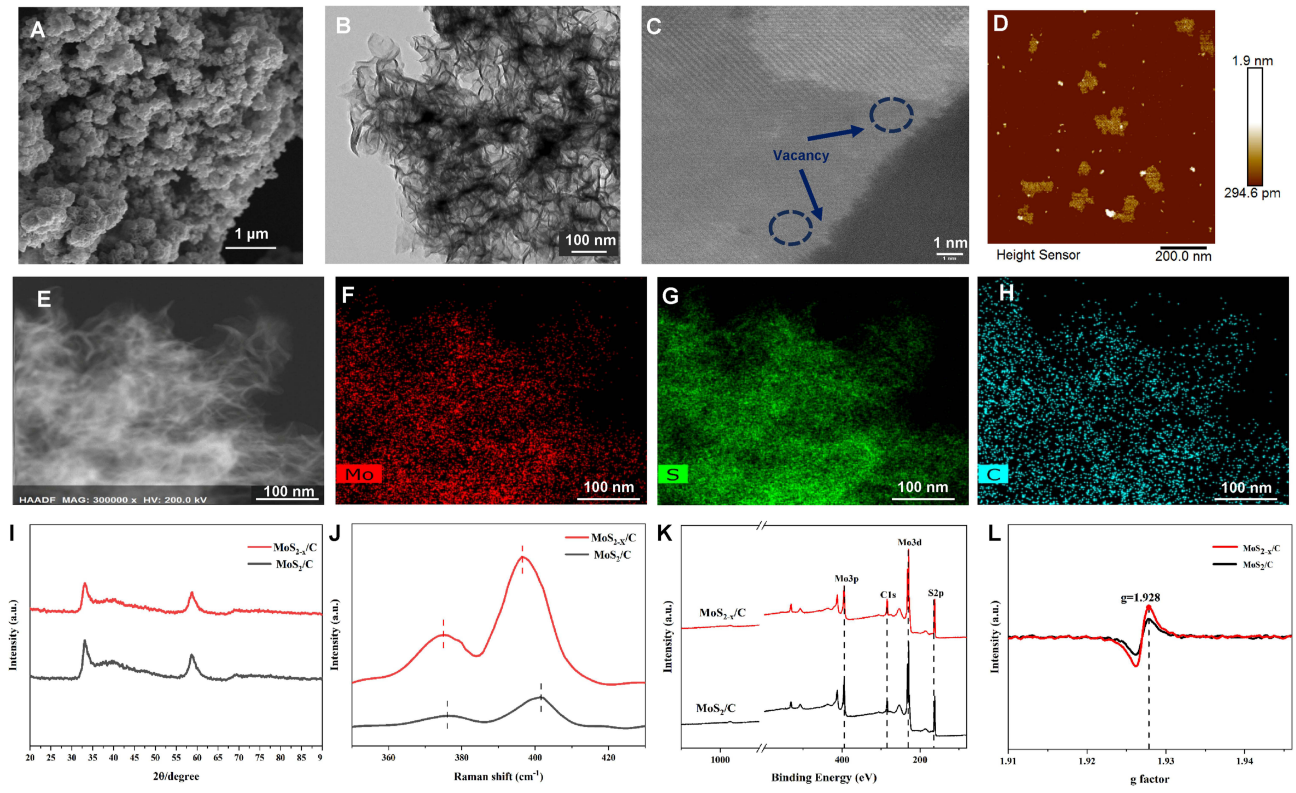

Figure 1 Morphology, structure and characterization of MoS_{2-x}/C NS. (**A**) SEM image, (**B**) TEM image, (**C**) HAADF-STEM images, the blue arrows and dashed circles represented the existence of sulfur vacancies. AFM image (**D**), HAADF-STEM image (**E**) and elemental mapping images of the MoS_{2-x}/C NS, including Mo (**F**), S (**G**), C (**H**) elements. XRD patterns (**I**), Raman spectra (**J**), XPS patterns (**K**), and EPR (**L**) results of MoS_2/C and MoS_{2-x}/C NS.

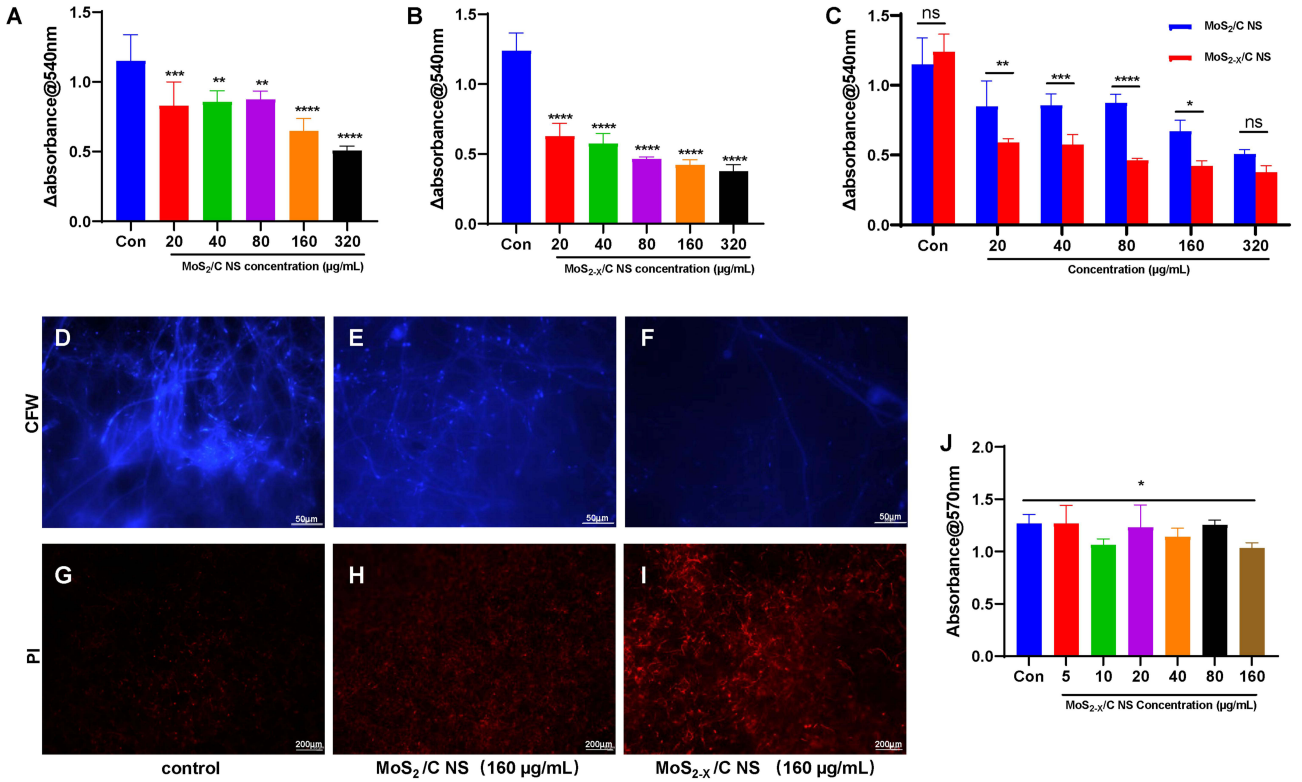

Figure 2 The antifungal ability of MoS_{2-x}/C NS against *A. fumigatus* is stronger than that of MoS_2/C NS because of the presence of sulfur vacancies. The inhibition of MoS_2/C NS (**A**) and MoS_{2-x}/C NS (**B**) on *A. fumigatus* spores (mean ± SD; one-way ANOVA). And the comparison (**C**) of MoS_2/C and MoS_{2-x}/C NS showed that the presence of sulfur vacancies enhanced antifungal ability under the concentration of 320 μg/mL (mean ± SD; two-way ANOVA). The CFW staining of hyphae demonstrated that compared to the control group (**D**), both MoS_2/C (**E**) and MoS_{2-x}/C NS (**F**) reduced the number of hyphae. PI staining showed that compared to the control group (**G**), both MoS_2/C NS (**H**) and MoS_{2-x}/C NS (**I**) treatment have increased fluorescence intensity in fungal hyphae. The crystal violet experiment (**J**) indicated that MoS_{2-x}/C NS inhibits biofilm formation of *A. fumigatus* (mean ± SD; one-way ANOVA). Δ, referred to the change of absorbance between the 0h and 24h time points.
Note: *$P < 0.05$, **$P < 0.01$, ***$P < 0.001$, ****$P < 0.0001$.
Abbreviations: ns, no significance.

MoS_2/C NS (Figure 2H) and MoS_{2-x}/C NS (Figure 2I) treatment groups exhibited red fluorescence. The MoS_{2-x}/C NS treatment group exhibited a higher intensity of red fluorescence, indicating that this treatment resulted in more significant damage to the cell membrane and demonstrated a superior antifungal effect. As well known, biofilms significantly cause the further invasion and drug resistance of fungus; therefore, the development of drugs targeting biofilm formation may facilitate the eradication of fungal infections.[42–44] We conducted crystal violet assays to evaluate the influence on the biofilm of *A. fumigatus*. The results indicated that MoS_{2-x}/C NS could inhibit biofilm formation (Figure 2J) at a concentration of 160 μg/mL, suggesting that MoS_{2-x}/C NS may reduce the drug resistance of this fungus. These results suggested that MoS_{2-x}/C NS possessed a greater capacity to inhibit spore growth and disrupt the cell membrane of *A. fumigatus*.

Toxicity Evaluation of MoS_{2-x}/C NS on HCECs and Mouse Corneas

To evaluate the biosafety of MoS_{2-x}/C NS, we employed an LDH detection kit to assess the impact of MoS_{2-x}/C NS on the viability of HCECs and investigated its damaging and irritating effects on mouse corneas through Draize eye toxicity experiment. In vitro, the cytotoxicity experiment indicated that the cell survival ability in the MoS_2/C NS (Figure 3A) and MoS_{2-x}/C NS (Figure 3B) treatment groups remained unaffected compared to the control group at concentrations of ≤160 μg/mL. Furthermore, the presence of sulfur vacancies did not result in increased cytotoxicity of MoS_2/C NS at concentrations not exceeding 160 μg/mL (Figure 3C). In vivo, the Draize eye toxicity test involved administering MoS_{2-x}/C NS dispersion at a concentration of 160 μg/mL to mice via eye drops for 5 days. Throughout this period, continuous dynamic observation of the mouse ocular surface was performed using ophthalmic slit lamps under cobalt blue lighting.

https://doi.org/10.2147/IJN.S552664

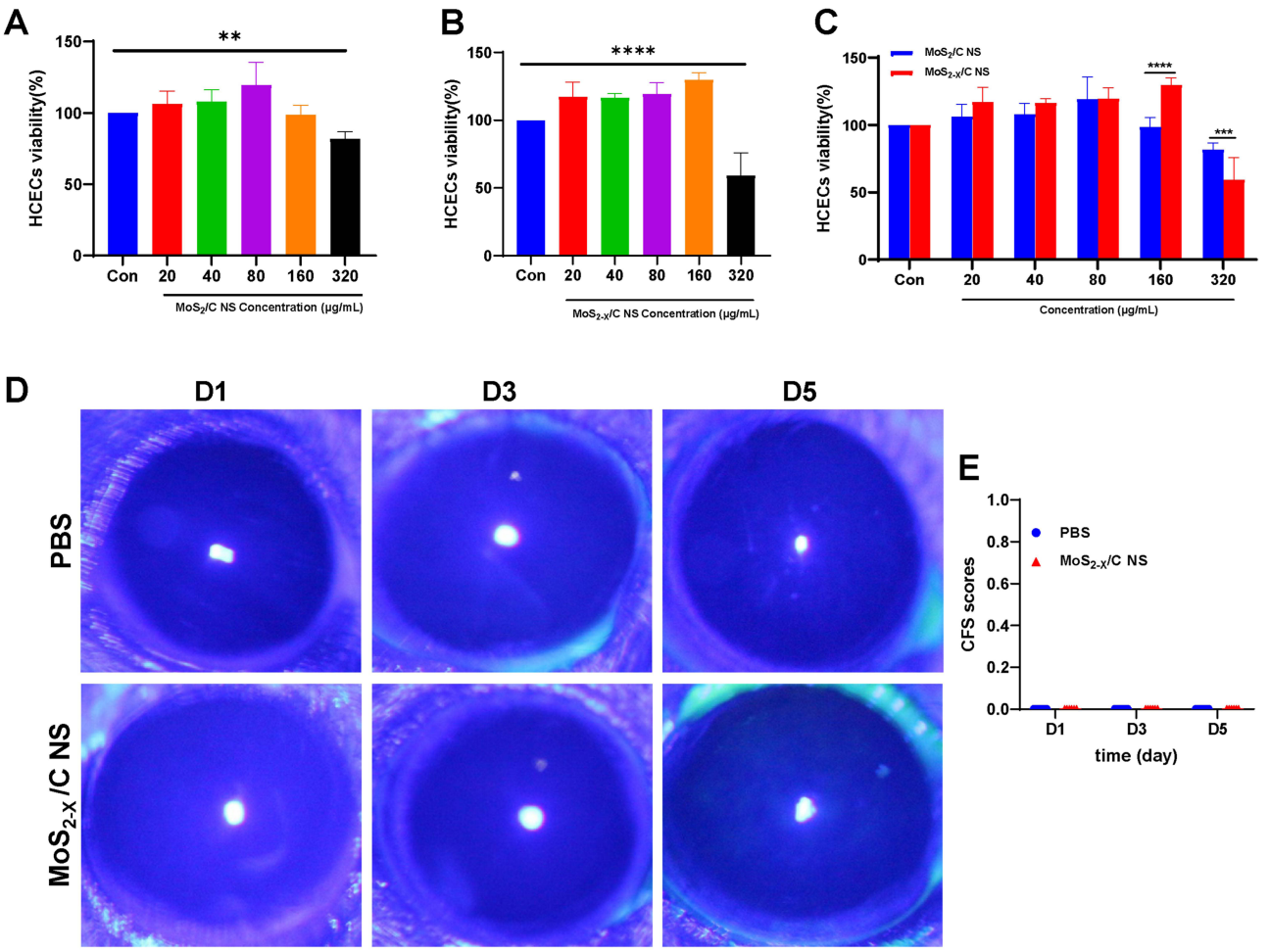

Figure 3 Safety assessment of MoS_{2-x}/C NS. The cell viability tests of MoS_2/C NS (**A**) and MoS_{2-x}/C NS (**B**) on HCECs was detected through LDH kit (mean ± SD; one-way ANOVA). The comparison (**C**) of MoS_{2-x}/C NS and MoS_2/C NS showed the production of sulfur vacancies does not increase the toxic effect of MoS_2/C NS on HCECs at the concentration below 320 μg/mL (mean ± SD; two-way ANOVA). The toxicity of MoS_{2-x}/C NS on mouse cornea was assessed by fluorescein staining (**D**). Corneal fluorescein staining (CFS) scores were evaluated (**E**).
Note: $^{**}P < 0.01$, $^{***}P < 0.001$, $^{****}P < 0.0001$.

The results demonstrated that, compared to the PBS group, MoS_{2-x}/C NS treatment did not induce any damage to the mouse cornea. Consistent with the PBS group, the MoS_{2-x}/C NS treatment group exhibited smooth corneal surfaces, intact corneal epithelium, and no fluorescein sodium staining (Figure 3D and E). The toxicity experiments indicated that MoS_{2-x}/C NS at a concentration of 160 μg/mL demonstrated good biocompatibility both in vivo and in vitro, aligning with previous research.[45–47] Furthermore, these results implied that sulfur vacancies enhanced the ability of MoS_2/C NS to inhibit *A. fumigatus* without causing significant toxic effects on cells. Consequently, MoS_{2-x}/C NS can be considered a safe, low-toxicity, and non-irritating nanomaterial for the cornea, exhibiting good biocompatibility. Moreover, 160 μg/mL was established as the safe and effective concentration of MoS_{2-x}/C NS for subsequent biological experiments.

Therapeutic Effects of MoS_{2-x}/C NS on *A. fumigatus* Keratitis

At 1, 3 and 5 days p.i., clinical scoring of *A. fumigatus* keratitis of mice was performed by evaluating the area, opacity, and morphology of corneal ulcers. Our results indicated that the PBS-treated group exhibited a larger corneal ulcer area and higher opacity, accompanied by neovascularization and corneal perforation at 3 and 5 days p.i. In contrast, the MoS_{2-x}/C NS treatment group demonstrated greater corneal transparency, reduced ulcer area, and absence of corneal neovascularization (Figure 4A). The clinical scores of keratitis in mice treated with MoS_{2-x}/C NS were lower than those in the PBS-treated group (Figure 4B). We collected corneas from the mice at the 3 days p.i. for plate counting and HE

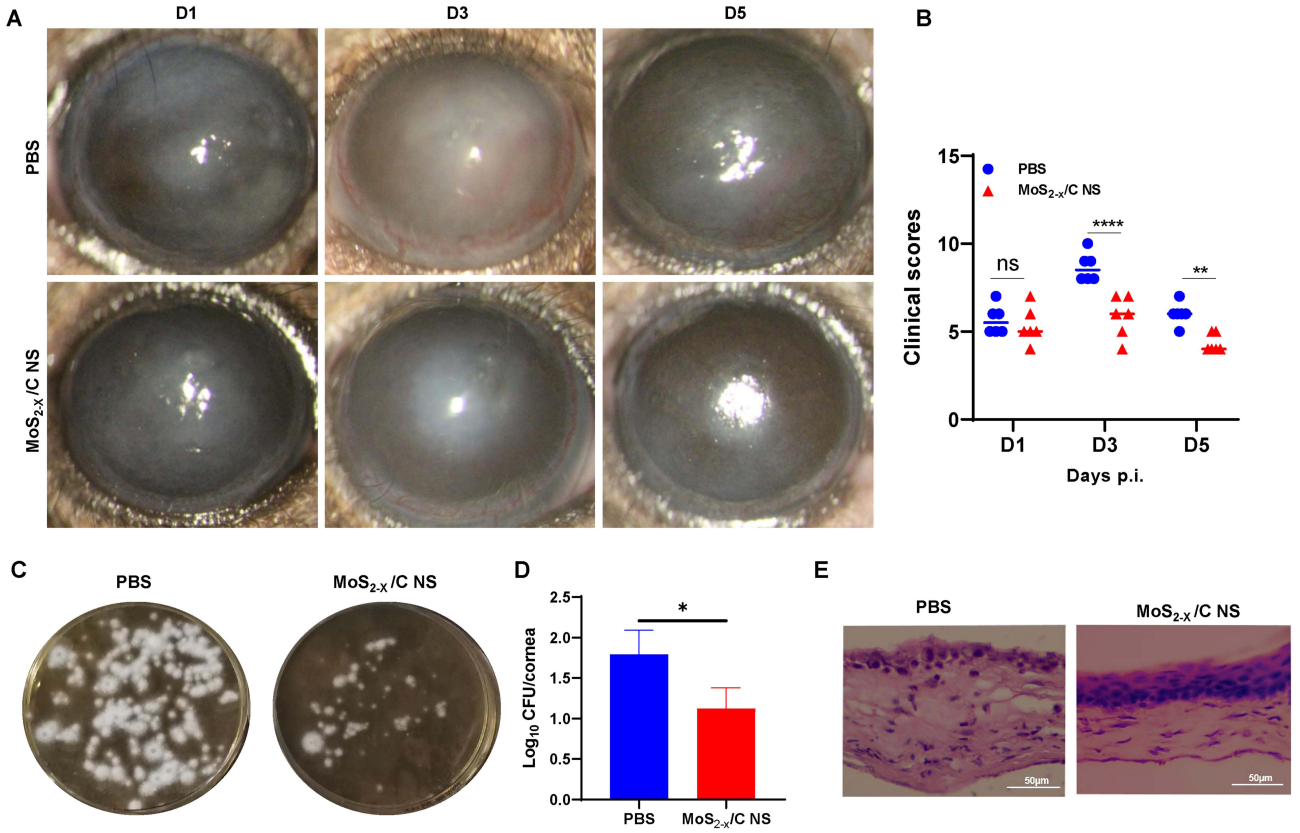

Figure 4 MoS_{2-x}/C NS improved the *A. fumigatus* keratitis in mice. On the 3rd and 5th days following *A. fumigatus* infection, the MoS_{2-x}/C NS treatment ameliorated mouse fungal keratitis (**A**) and lowered clinical scores (**B**, mean ± SD; two-way ANOVA) compared to the PBS treatment group. Corneas were collected from mice on the 3rd day p.i. for plate colony counting and HE staining. MoS_{2-x}/C NS treatment reduced fungal colonies numbers (**C** and **D**) in the infected corneas (mean ± SD; *t*-test). Furthermore, MoS_{2-x}/C NS treatment reduced the infiltration of inflammatory cells within the infected corneal tissue, alongside alleviation of tissue edema and damage (**E**).
Note: *$P < 0.05$, **$P < 0.01$, **** $P < 0.0001$.
Abbreviations: ns, no significance.

staining. Plate counting revealed a higher number of fungal colonies cultured from the corneal homogenate of mice treated with PBS, indicating a greater residual fungal presence in the corneal tissue. Conversely, the number of fungal colonies cultured from the corneal homogenate of mice in the MoS_{2-x}/C NS treatment group was significantly reduced, suggesting a decrease in the residual fungal count in the corneas (Figure 4C and D). As previously mentioned, the fungal load influenced fungal invasiveness.[48] Our findings indicated that treatment with MoS_{2-x}/C NS diminished the fungal load of the infected corneas, suggesting that MoS_{2-x}/C NS inhibited further fungal invasion by reducing the residual fungal count in the corneas. HE staining (Figure 4E) indicated that in the control group, a substantial number of inflammatory cells aggregated and infiltrated in the stromal layer of the cornea, primarily concentrating at the site of the infected ulcer. In contrast, the MoS_{2-x}/C NS treatment reduced the infiltration of inflammatory cell and improved pathological structure of *A. fumigatus*-infected corneas.

MoS_{2-x}/C NS Reduced the Expression Levels of Pro-Inflammatory Factors Induced by *A. fumigatus*

The pathophysiological process of fungal keratitis is both complex and intriguing. From the fungal perspective, spores through the damaged corneal epithelium and invade the corneal stroma through adhesion, where they germinate and produce hyphae. The proliferation of these fungal hyphae not only inflicts physical damage on the corneal structure but also generates toxic factors, including extracellular enzymes that enhance the fungi's invasiveness. Furthermore, fungus can secrete proteases that induce the production of pro-inflammatory factors and recruit neutrophils, leading to additional tissue damage, reduced corneal transparency, and vision loss.[49–52] From the host's perspective, when fungi invade the

cornea, immune cells become activated, releasing inflammatory mediators and recruiting neutrophils to eliminate the fungus. However, excessive inflammatory response can be detrimental to normal corneal tissue. If this inflammatory response is not promptly and effectively managed, it may result in permanent tissue damage to the cornea. Researches have indicated that controlling the excessive inflammatory response can be beneficial in the treatment of fungal keratitis.[53–55] Therefore, it is particularly important to identify new strategies that can rapidly and effectively eradicate pathogenic fungi while minimizing excessive corneal inflammatory damage in the treatment of fungal keratitis. Therefore, we studied the anti-inflammatory properties of MoS_{2-x}/C NS in fungal keratitis both in vitro and in vivo.

Our studies indicated that after stimulated by inactivated hyphae of *A. fumigatus*, the expression levels of pro-inflammatory factors of HCECs were significantly elevated. However, MoS_{2-x}/C NS treatment effectively reduced the expression of TNF-α (Figure 5A) and IL-6 (Figure 5B) induced by *A. fumigatus* stimulation. Additionally, a study by Hua et al indicated that exposure of HCECs to *Candida albicans* increased ROS production, exacerbating the pathological process of fungal keratitis through oxidative stress and activation of p38/MAPK signaling pathway.[56] Consequently, we proposed that ROS represented a promising target for the treatment of fungal keratitis. Nanoscale MoS_2, recognized for its excellent antioxidant properties, has the capacity to scavenge various types of free radicals.[57–59] Researches indicated that MoS_2 could diminish the levels of pro-inflammatory factors in human bronchial cells and microglia, exhibiting remarkable antioxidant stress and anti-inflammatory protective capabilities.[60–64] These findings are consistent with our research results. In our experiments, H_2O_2, used as a positive inducer of ROS, allows for the assessment of true intracellular ROS levels in various treatment groups by analyzing the fluorescence signal intensity from the positive control group. As illustrated in Figure 5D, the group stimulated by the inactivated mycelium of *A. fumigatus* showed increased ROS production and higher green fluorescence intensity in the cells surrounding the mycelium. Notably, the green fluorescence intensity in the MoS_{2-x}/C NS treatment group decreased, indicating that MoS_{2-x}/C NS treatment effectively mitigates excess ROS produced in HCECs stimulated by inactivated hyphae of *A. fumigatus* (Figure 5C). These results indicated that MoS_{2-x}/C NS reduced ROS, thereby alleviating the oxidative stress response. In vivo, the expression of the pro-inflammatory factors IL-6 and TNF-α in the corneas of fungal keratitis mice treated with PBS were significantly elevated. In contrast, the levels of IL-6 (Figure 5E) and TNF-α (Figure 5F) in the MoS_{2-x}/C NS treatment group were lower than those in PBS treatment group.

MoS_{2-x}/C NS Promoted Migration of HCECs

In addition to exerting an antifungal effect and reducing the inflammatory response, studies have demonstrated that MoS_2 possesses a notable ability to promote wound healing in infectious wounds, potentially by enhancing fibroblast migration and proliferation.[65,66] The human placental amniotic membrane has extensive applications in ophthalmic surgery. Notably, a previous study showed that loading polycaprolactone (PCL) hybridized MoS_2 onto decellularized human placental amniotic membrane scaffolds can reduce inflammation at the anastomotic site following colon surgery in rats, thereby promoting anastomotic healing.[67] To investigate the effect of MoS_{2-x}/C NS on corneal epithelial migration ability, we conducted scratch assays. Our results indicated that the scratch area of HCECs was significantly reduced after treatment with MoS_{2-x}/C NS for 24 hours (Figure 6A). As shown in Figure 6B, MoS_{2-x}/C NS treatment increased the cell migration rate, suggesting that MoS_{2-x}/C NS treatment promotes the migration of HCECs. We believe this effect is closely associated with the presence of the molybdenum element. He et al firstly demonstrated that molybdenum-containing materials could target macrophages and exert immunomodulatory effects within the dynamic cascade of wound healing.[68] Combined our experimental results, these findings supply new insights for the design of molybdenum-containing materials in tissue engineering and regenerative medicine.

Limitations and Future Perspectives

Although this study demonstrates the excellent dual functionalities of MoS_{2-x}/C NS, several limitations of the research must be acknowledged. Firstly, the current work has not yet systematically explored the impact of sulfur vacancy concentration on antifungal and anti-inflammatory capabilities. Research on bacterial keratitis has indicated that a specific density of sulfur vacancies is crucial for enhancing catalytic and antibacterial activity; however, an excess of vacancies may form charge carrier recombination centers, potentially compromising electronic properties and reducing

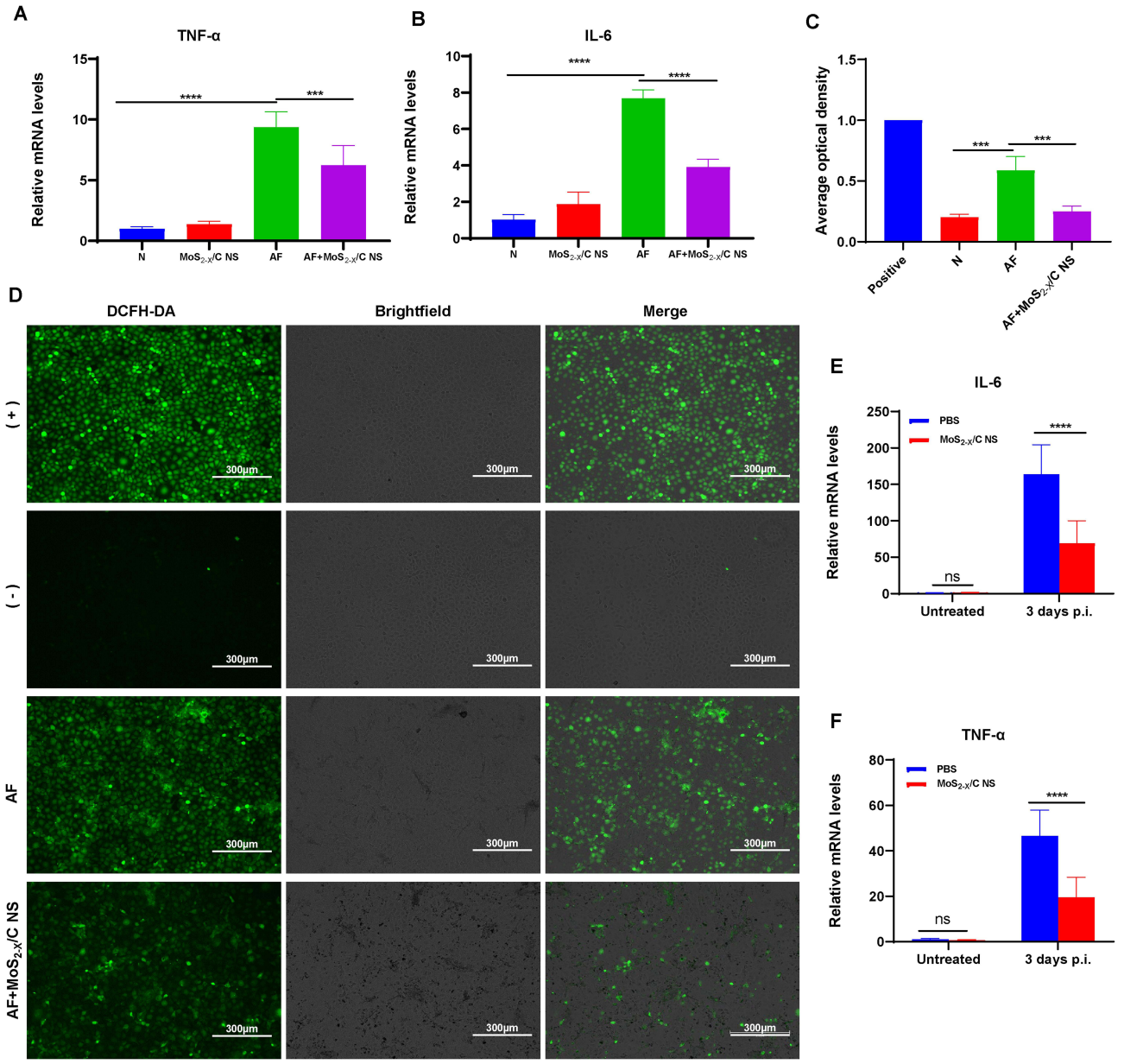

Figure 5 MoS_{2-x}/C NS demonstrated anti-inflammatory effects. In vitro, MoS_{2-x}/C NS reduced the expression levels of TNF-α (**A**) and IL-6 (**B**) in HCECs stimulated by inactivated mycelium of *A. fumigatus* (mean ± SD; one-way ANOVA). When using the fluorescent probe DCFH-A to label ROS, a substantial green fluorescence signal was tested in H_2O_2 positive control group (**D**). The fluorescence quantitative analysis ((**C**), mean ± SD; one-way ANOVA) showed that in comparison to normal group, HCECs stimulated by inactivated *A. fumigatus* exhibited an increased green fluorescence signal. However, following treatment with MoS_{2-x}/C NS, a reduction in fluorescence signal was noted. In vivo, after 3 days of treatment with MoS_{2-x}/C NS, the expressions of IL-6 (**E**) and TNF-α (**F**) in infected corneal tissue of mice with *A. fumigatus* keratitis were lower than those in PBS-treated group (mean ± SD; *t*-test).

Note: *** $P < 0.001$, **** $P < 0.0001$.

Abbreviations: ns, no significance.

antibacterial efficacy.[69] Secondly, compared with existing literature on antimicrobial applications of MoS_2 nanomaterials, previous research has predominantly focused on their intrinsic antibacterial properties, such as the inhibition of *Staphylococcus aureus*[15] and anti-inflammatory effects[70,71] of drug-loaded MoS_2. Our study advances the field by constructing sulfur vacancies, which not only enhance the antifungal activity but also concurrently explore the anti-inflammatory capabilities of MoS_{2-x}/C NS, which is a crucial combination strategy for treating fungal keratitis. Finally, further investigation and exploration in other fungal pathogens such as *Candida albicans* are necessary, as *Candida albicans* is also a major pathogen of fungal keratitis.

https://doi.org/10.2147/IJN.S552664

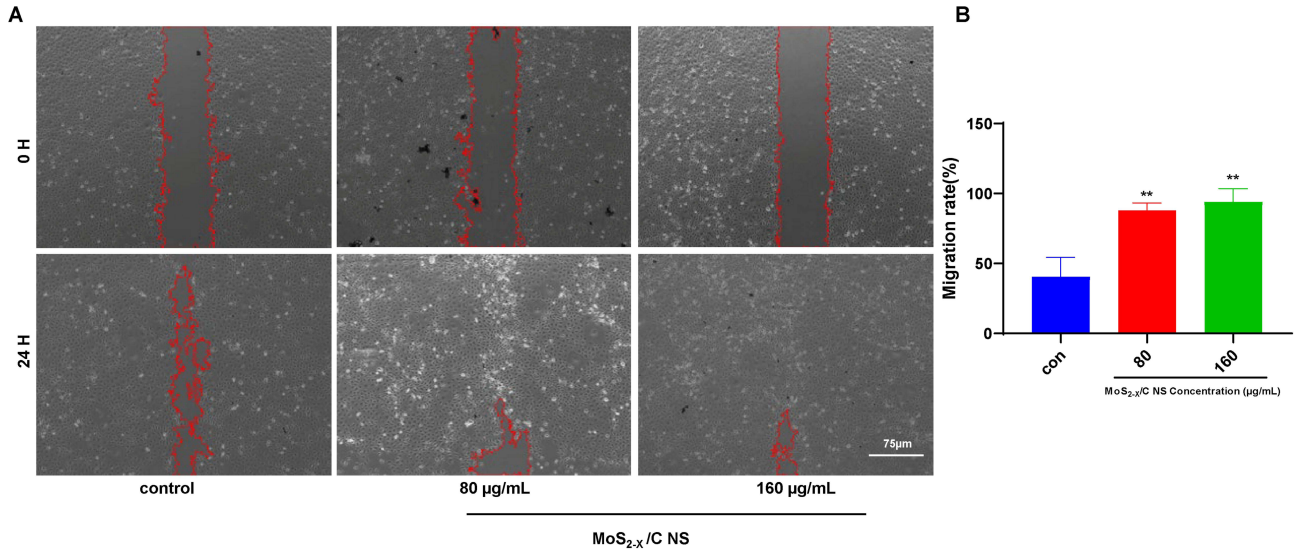

Figure 6 MoS_{2-x}/C NS enhanced the migratory ability of HCECs. The images of the cell scratch assay (**A**) and the corresponding quantitative analysis ((**B**), mean ± SD; one-way ANOVA) showed that compared to the control group, MoS_{2-x}/C NS significantly reduced the scratch area in a concentration-dependent. The red lines indicated the scratch edge of the HCECs when we measured the scratch distance generated by ImageJ software to measure the scratch distance.
Note: $^{**}P < 0.01$.

Future research will focus on two directions: at the fundamental level, elucidating the specific molecular pathways of the antifungal and anti-inflammatory effects; and from a translational perspective, optimizing advanced delivery systems (such as thermosensitive gels) by integrating release and stability data to enhance corneal residence time and ultimately improve clinical efficacy.

Conclusion

Fungal keratitis remains a challenging ocular infection with limited therapeutic effect due to poor drug penetration, fungal resistance, and excessive inflammatory damage.[72–74] This study demonstrates that MoS_{2-x}/C NS, engineered with sulfur vacancies, represents an effective dual-functional nanomaterial for its management. Our findings confirmed its simultaneous antifungal activity against *A. fumigatus* and anti-inflammatory effects, which collectively reduced fungal load, suppressed excessive inflammation, and promoted corneal epithelial repair of *A. fumigatus* keratitis. The material's capacity to address both pathogenic clearance and immune regulation underscores its therapeutic advantage. This work highlights the potential of vacancy-engineered nanomaterial as a comprehensive therapeutic strategy for fungal keratitis. Future research will focus on elucidating the detailed molecular mechanisms and optimizing delivery systems to enhance clinical translatability.

Acknowledgment

This work was supported by the National Natural Science Foundation of China (Nos. 81800800, 82171029 and 81870632), the Taishan Scholars Program (Nos. tsqn202103188).

Disclosure

The authors report no conflicts of interest in this work.

References

1. Ung L, Acharya NR, Agarwal T, et al. Infectious corneal ulceration: a proposal for neglected tropical disease status. *Bulletin of the World Health Organization*. 2019;97(12):854–856. doi:10.2471/blt.19.232660
2. Cabrera-Aguas M, Khoo P, Watson SL. Infectious keratitis: a review. *Clin Exp Ophthalmol*. 2022;50(5):543–562. doi:10.1111/ceo.14113
3. Arboleda A, Ta CN. Overview of mycotic keratitis. *Cornea*. 2024;43(9):1065–1071. doi:10.1097/ico.0000000000003559

4. Watson SL, Cabrera-Aguas M, Keay L, Khoo P, McCall D, Lahra MM. The clinical and microbiological features and outcomes of fungal keratitis over 9 years in Sydney, Australia. *Mycoses*. 2020;63(1):43–51. doi:10.1111/myc.13009
5. Putri RA, Enggi CK, Sulistiawati S, et al. Development of itraconazole ocular delivery system using β-cyclodextrin complexation incorporated into dissolving microneedles for potential improvement treatment of fungal keratitis. *J biomater sci Poly ed*. 2024;35(15):2315–2342. doi:10.1080/09205063.2024.2380129
6. Gungor B, Erdogan H, Suner SS, Silan C, Saraydin SU, Sahiner N. Drug-impregnated contact lenses via supercritical carbon dioxide: a viable solution for the treatment of bacterial and fungal keratitis. *Int J Pharm*. 2024;662:124505. doi:10.1016/j.ijpharm.2024.124505
7. Huang T, Li X, Maier M, NM O-S, Heath DE, O'Connor AJ. Using inorganic nanoparticles to fight fungal infections in the antimicrobial resistant era. *Acta Biomater*. 2023;158:56–79. doi:10.1016/j.actbio.2023.01.019
8. Courtney CM, Goodman SM, McDaniel JA, Madinger NE, Chatterjee A, Nagpal P. Photoexcited quantum dots for killing multidrug-resistant bacteria. *Nature Mater*. 2016;15(5):529–534. doi:10.1038/nmat4542
9. Yoonhee So DY, Lee S, Lee H, et al. Insights into the selective bactericidal activity of W(Mo)Se2 nanosheets for therapy of pathogenic bacterial infections. *Chem Eng J*. 2023;468. doi:10.1016/j.cej.2023.143727
10. Debnath A, Saha S, Li DO, et al. Elimination of multidrug-resistant bacteria by transition metal dichalcogenides encapsulated by synthetic single-stranded DNA. *ACS Appl. Mater. Interfaces*. 2021;13(7):8082–8094. doi:10.1021/acsami.0c22941
11. Nan H, Zhou R, Gu X, Xiao S, Ken Ostrikov K. Recent advances in plasma modification of 2D transition metal dichalcogenides. *Nanoscale*. 2019;11(41):19202–19213. doi:10.1039/c9nr05522c
12. Bharti S, Tripathi SK, Singh K. Recent progress in MoS(2) nanostructures for biomedical applications: experimental and computational approach. *Anal. Biochem*. 2024;685:115404. doi:10.1016/j.ab.2023.115404
13. Joorabloo A, Liu T. Recent advances in reactive oxygen species scavenging nanomaterials for wound healing. *Exploration*. 2024;4(3):20230066. doi:10.1002/exp.20230066
14. Yang Z, You J, Zhai S, et al. pH-responsive molybdenum disulphide composite nanomaterials for skin wound healing using "ROS leveraging" synergistic immunomodulation. *Mater Today Bio*. 2025;31:101481. doi:10.1016/j.mtbio.2025.101481
15. Zhang W, Kuang Z, Song P, et al. Synthesis of a two-dimensional molybdenum disulfide nanosheet and ultrasensitive trapping of staphylococcus aureus for enhanced photothermal and antibacterial wound-healing therapy. *Nanomaterials*. 2022;12(11). doi:10.3390/nano12111865
16. Lu Y, Kang W, Yu Y, et al. Antibacterial and antioxidant bifunctional hydrogel based on hyaluronic acid complex MoS(2)-dithiothreitol nanozyme for treatment of infected wounds. *Regenerative Biomaterials*. 2024;11:rbae025. doi:10.1093/rb/rbae025
17. Alikarami M, Saremi H, Darvishnia M. Sustainable antifungal potential of ZnO and MoS(2) nanoparticles against Fusarium oxysporum and Fusarium graminearum. *World J Microbiol Biotechnol*. 2025;41(8):312. doi:10.1007/s11274-025-04531-3
18. Basu P, Chakraborty J, Ganguli N, et al. Defect-engineered mos(2) nanostructures for reactive oxygen species generation in the dark: antipollutant and antifungal performances. *ACS Appl. Mater. Interfaces*. 2019;11(51):48179–48191. doi:10.1021/acsami.9b12988
19. Thayil R, Krishna KG, Chinthamreddy A, Parne SR. Exploring the multifunctionality of MoS2 and MoSe2 nanostructures: enhanced ammonia sensing, antimicrobial activity and organic dye adsorption. *Microchem J*. 2024;204. doi:10.1016/j.microc.2024.111175
20. Zalneravicius R, Klimas V, Paskevicius A, et al. Highly efficient antimicrobial agents based on sulfur-enriched, hydrophilic molybdenum disulfide nano/microparticles and coatings functionalized with palladium nanoparticles. *J Colloid Interface Sci*. 2021;591:115–128. doi:10.1016/j.jcis.2021.01.103
21. Zhang W, Yang L, Li H, et al. Synthesis of 2D molybdenum disulfide nanoplatform with effective chemo-photothermal antifungal activities and extended shelf-life of fruits. *Mater Chem Phys*. 2023:296. doi:10.1016/j.matchemphys.2023.127350.
22. Lima T, Gunnarsson SB, Coelho E, et al. β-glucan-functionalized nanoparticles down-modulate the proinflammatory response of mononuclear phagocytes challenged with candida albicans. *Nanomaterials*. 2022;12(14):2475. doi:10.3390/nano12142475
23. Yu B, Li C, Gu L, et al. Eugenol protects against Aspergillus fumigatus keratitis by inhibiting inflammatory response and reducing fungal load. *Eur. J. Pharmacol*. 2022;924:174955. doi:10.1016/j.ejphar.2022.174955
24. Niu P, Wu Y, Zeng F, Zhang S, Liu S, Gao H. Development of nanodrug-based eye drops with good penetration properties and ROS responsiveness for controllable release to treat fungal keratitis. *NPG Asia Materials*. 2023;15(1):31. doi:10.1038/s41427-023-00478-9
25. Fortingo N, Melnyk S, Sutton SH, Watsky MA, Bollag WB. Innate immune system activation, inflammation and corneal wound healing. *Int J Mol Sci*. 2022;23(23):14933. doi:10.3390/ijms232314933
26. Liu X, Sui J, Li C, et al. The preparation and therapeutic effects of β-glucan-specific nanobodies and nanobody-natamycin conjugates in fungal keratitis. *Acta Biomater*. 2023;169:398–409. doi:10.1016/j.actbio.2023.08.019
27. Peng Y, Pang S, Zeng Y, et al. Antibiotic-free ocular sterilization while suppressing immune response to protect corneal transparency in infectious keratitis treatment. *J Control Release*. 2024;374:563–576. doi:10.1016/j.jconrel.2024.08.038
28. Gu L, Lin J, Wang Q, et al. Mesoporous zinc oxide-based drug delivery system offers an antifungal and immunoregulatory strategy for treating keratitis. *J Control Release*. 2024;368:483–497. doi:10.1016/j.jconrel.2024.03.006
29. Chen T, Zou H, Wu X, et al. Fullerene-like MoS(2) nanoparticles as cascade catalysts improving lubricant and antioxidant abilities of artificial synovial fluid. *ACS Biomater. Sci. Eng*. 2019;5(6):3079–3088. doi:10.1021/acsbiomaterials.9b00372
30. Ren C, Li D, Zhou Q, Hu X. Mitochondria-targeted TPP-MoS(2) with dual enzyme activity provides efficient neuroprotection through M1/M2 microglial polarization in an Alzheimer's disease model. *Biomaterials*. 2020;232:119752. doi:10.1016/j.biomaterials.2019.119752
31. Ma D, Wang LP, et al. S-vacancies manipulating enhances Na<insertion of MoS_2 for efficient sodium-ion storage. *Chem Eng J*. 2023:457. doi:10.1016/j.cej.2022.141116.
32. Tian Z, Tan TT, Hu YW, et al. 7,8-Dihydroxyflavone attenuates cisplatin-induced cardiomyocyte apoptosis and mitochondrial dysfunction via the p53/Nrf2 pathway. *Toxicol Appl Pharmacol*. 2025;505:117578. doi:10.1016/j.taap.2025.117578
33. Elhabal SF, Faheem AM, Hababeh S, et al. Dissolving microneedles containing lactoferrin nanosuspension for enhancement of antimicrobial and anti-inflammatory effects in the treatment of dry eye disease. *Pharmaceutics*. 2025;17(5):653. doi:10.3390/pharmaceutics17050653
34. Huang M, Yan X, Gao Y, et al. The effect of type 2 diabetes mellitus on lid wiper epitheliopathy and ocular surface parameters. *Heliyon*. 2024;10(17):e36912. doi:10.1016/j.heliyon.2024.e36912
35. Kamran M, Aftab M, Amir A, et al. Synthesis and evaluation of a chitosan-based cationic hydrogel with strong antifungal and antibiofilm activities against clinical isolates of candida auris. *Pharmaceuticals*. 2025;18(4):506. doi:10.3390/ph18040506

36. de Melo Silva VG, de Sousa BR, De santana DL, et al. Novel aryloxy-hydrazone-thiazoles: design, synthesis, ADMET prediction and antifungal activity against Sporothrix spp. *Chem. Biol. Interact*. 2025;421(421):111715. doi:10.1016/j.cbi.2025.111715
37. Kader M, Xu L, Fang L, et al. The antimicrobial extract derived from pseudomonas sp. HP-1 for inhibition of aspergillus flavus growth and prolongation of maize seed storage. *Foods*. 2025;14(10):1774. doi:10.3390/foods14101774
38. Wu TG, Wilhelmus KR, Mitchell BM. Experimental keratomycosis in a mouse model. *Invest Ophthalmol Visual Sci*. 2003;44(1):210–216. doi:10.1167/iovs.02-0446
39. Wu J, Wang W, Yuan F, et al. CXCL16 exacerbates Pseudomonas aeruginosa keratitis by promoting neutrophil activation. *Int Immunopharmacol*. 2024;127:111375. doi:10.1016/j.intimp.2023.111375
40. Gu L, Li C, Lin J, et al. Drug-loaded mesoporous carbon with sustained drug release capacity and enhanced antifungal activity to treat fungal keratitis. *Biomater Adv*. 2022;136:212771. doi:10.1016/j.bioadv.2022.212771
41. Liu Z, Ma F, Wu B, et al. Multifunctional methacrylated gelatin-hyaluronic acid-psoralen hydrogel for bone defect repair: synergistic anti-inflammatory, ROS-scavenging, and osteoinductive effects. *Int J Biol Macromol*. 2025;330:147838. doi:10.1016/j.ijbiomac.2025.147838
42. Wang Z, Lin J, Wang Q, et al. Rosmarinic acid alleviates fungal keratitis caused by Aspergillus fumigatus by inducing macrophage autophagy. *Exp. Eye Res*. 2024;244:109944. doi:10.1016/j.exer.2024.109944
43. Ye Y, He J, Wang H, et al. Cell wall destruction and internal cascade synergistic antifungal strategy for fungal keratitis. *ACS nano*. 2022;16 (11):18729–18745. doi:10.1021/acsnano.2c07444
44. He J, Ye Y, Zhang D, Yao K, Zhou M. Visualized gallium/lyticase-integrated antifungal strategy for fungal keratitis treatment. *Adv. Mater*. 2022;34 (49):e2206437. doi:10.1002/adma.202206437
45. Appel JH, Li DO, Podlevsky JD, et al. Low cytotoxicity and genotoxicity of two-dimensional moS(2) and WS(2). *ACS Biomater. Sci. Eng*. 2016;2 (3):361–367. doi:10.1021/acsbiomaterials.5b00467
46. Zhou K, Zhang Y, Xia Z, Wei W. As-prepared MoS2 quantum dot as a facile fluorescent probe for long-term tracing of live cells. *Nanotechnology*. 2016;27(27):275101. doi:10.1088/0957-4484/27/27/275101
47. Zhang XD, Zhang J, Wang J, et al. Highly catalytic nanodots with renal clearance for radiation protection. *ACS nano*. 2016;10(4):4511–4519. doi:10.1021/acsnano.6b00321
48. Vemuganti GK, Garg P, Gopinathan U, et al. Evaluation of agent and host factors in progression of mycotic keratitis: a histologic and microbiologic study of 167 corneal buttons. *Ophthalmology*. 2002;109(8):1538–1546. doi:10.1016/s0161-6420(02)01088-6
49. Hohl TM, Feldmesser M. Aspergillus fumigatus: principles of pathogenesis and host defense. *Eukaryotic Cell*. 2007;6(11):1953–1963. doi:10.1128/ec.00274-07
50. Yike I. Fungal proteases and their pathophysiological effects. *Mycopathologia*. 2011;171(5):299–323. doi:10.1007/s11046-010-9386-2
51. Park M, Do E, Jung WH. Lipolytic enzymes involved in the virulence of human pathogenic fungi. *Mycobiology*. 2013;41(2):67–72. doi:10.5941/myco.2013.41.2.67
52. Mellon JE, Cotty PJ, Dowd MK. Aspergillus flavus hydrolases: their roles in pathogenesis and substrate utilization. *Appl. Microbiol. Biotechnol*. 2007;77(3):497–504. doi:10.1007/s00253-007-1201-8
53. Zhou H, Zhang H, Bi M, Zhang W. The role of PPAR in fungal keratitis. *Front Immunol*. 2024;15:1454463. doi:10.3389/fimmu.2024.1454463
54. Han F, Wang L, Wu J, et al. Inhibition of LRRK2 ameliorates aspergillus fumigatus keratitis by regulating sting signaling pathways. *Invest Ophthalmol Visual Sci*. 2025;66(2):13. doi:10.1167/iovs.66.2.13
55. Yang J, Zhong J, Fu Z, He D, Zhang J, Yuan J. Piezo1 enhances macrophage phagocytosis and pyrin activation to ameliorate fungal keratitis. *Invest Ophthalmol Visual Sci*. 2025;66(1):33. doi:10.1167/iovs.66.1.33
56. Hua X, Chi W, Su L, Li J, Zhang Z, Yuan X. ROS-induced oxidative injury involved in pathogenesis of fungal keratitis via p38 MAPK activation. *Sci Rep*. 2017;7(1):10421. doi:10.1038/s41598-017-09636-w
57. Presutti D, Agarwal T, Zarepour A, et al. Transition Metal Dichalcogenides (TMDC)-based nanozymes for biosensing and therapeutic applications. *Materials*. 2022;15(1). doi:10.3390/ma15010337
58. Xu J, Cai R, Zhang Y, Mu X. Molybdenum disulfide-based materials with enzyme-like characteristics for biological applications. *Colloids Surf. B*. 2021;200:111575. doi:10.1016/j.colsurfb.2021.111575
59. Yim D, Kim JE, Kim HI, et al. Adjustable intermolecular interactions allowing 2d transition metal dichalcogenides with prolonged scavenging activity for reactive oxygen species. *Small*. 2018;14(16):e1800026. doi:10.1002/smll.201800026
60. Pardo M, Shuster-Meiseles T, Levin-Zaidman S, Rudich A, Rudich Y. Low cytotoxicity of inorganic nanotubes and fullerene-like nanostructures in human bronchial epithelial cells: relation to inflammatory gene induction and antioxidant response. *Environ. Sci. Technol*. 2014;48(6):3457–3466. doi:10.1021/es500065z
61. Chen T, Zou H, Wu X, et al. Nanozymatic Antioxidant System Based on MoS(2) Nanosheets. *ACS Appl. Mater. Interfaces*. 2018;10 (15):12453–12462. doi:10.1021/acsami.8b01245
62. Alomari OA, Qusti S, Balgoon M, Aljoud F, Alamry KA, Hussein MA. Modified TPP-MoS(2) QD Blend as a Bio-Functional Model for Normalizing Microglial Dysfunction in Alzheimer's Disease. *Neurol Int*. 2023;15(3):954–966. doi:10.3390/neurolint15030061
63. Li Y, Tang H, Zhu H, et al. Ultrasmall molybdenum disulfide quantum dots cage alzheimer's amyloid beta to restore membrane fluidity. *ACS Appl. Mater. Interfaces*. 2021;13(25):29936–29948. doi:10.1021/acsami.1c06478
64. Han Q, Cai S, Yang L, et al. Molybdenum disulfide nanoparticles as multifunctional inhibitors against alzheimer's disease. *ACS Appl. Mater. Interfaces*. 2017;9(25):21116–21123. doi:10.1021/acsami.7b03816
65. Wang Y, Liu K, Huang K, Wei W, Huang Y, Dai H. Photothermal antibacterial MoS(2) composited chitosan hydrogel for infectious wound healing. *Biomater Adv*. 2024;156:213701. doi:10.1016/j.bioadv.2023.213701
66. Mu Z, Jin T, Chu T, et al. Functionalized MoS(2)-nanosheets with NIR-Triggered nitric oxide delivery and photothermal activities for synergistic antibacterial and regeneration-promoting therapy. *J Nanobiotechnol*. 2023;21(1):463. doi:10.1186/s12951-023-02167-9
67. Ebrahim Soltani Z, Elahi M, Tashak-Golroudbari H, et al. Evaluation of colonic anastomosis healing using hybrid nanosheets containing molybdenum disulfide (MOS2) scaffold of human placental amniotic membrane and polycaprolactone (PCL) in rat animal model. *Naunyn-Schmiedeberg's Arch Pharmacol*. 2023;396(9):1911–1921. doi:10.1007/s00210-023-02438-0
68. He XT, Li X, Zhang M, et al. Role of molybdenum in material immunomodulation and periodontal wound healing: targeting immunometabolism and mitochondrial function for macrophage modulation. *Biomaterials*. 2022;283:121439. doi:10.1016/j.biomaterials.2022.121439

69. Li H, Wang X, Zhao X, et al. Vacancy-Induced Antibacterial Activity of XS(2-)(y) quantum dots against drug-resistant bacteria for treatment of bacterial keratitis. *Small*. 2020;16(42):e2004677. doi:10.1002/smll.202004677
70. Chen CK, Chiu HW, Nguyen HT, Lu HT, Chuang AE. Transdermally administered nanozymes-infused F127/methylcellulose hydrogel for osteoarthritis relief via immunomodulatory pathways. *Int J Biol Macromol*. 2025;314:144114. doi:10.1016/j.ijbiomac.2025.144114
71. Lal DK, Kumar B, Kaushik V, Alhowyan A, Kalam MA. Molybdenum disulfide nanosheet-based nanocomposite for the topical delivery of umbelliferone: evaluation of anti-inflammatory and analgesic potentials. *ACS omega*. 2024;9(35):37105–37116. doi:10.1021/acsomega.4c04252
72. Sun S, Lui Q, Han L, et al. Identification and characterization of fusarium proliferatum, a new species of fungi that cause fungal keratitis. *Sci Rep*. 2018;8(1):4859. doi:10.1038/s41598-018-23255-z
73. Chaiwut C, Tadtong S, Akachaipaibul P, et al. Thermosensitive In situ ophthalmic gel for effective local delivery and antifungal activity of ketoconazole nanoparticles. *Gels*. 2024;11(1):13. doi:10.3390/gels11010013
74. Qu S, Zheng S, Muhammad S, Huang L, Guo B. An exploration of the ocular mysteries linking nanoparticles to the patho-therapeutic effects against keratitis. *J Nanobiotechnol*. 2025;23(1):184. doi:10.1186/s12951-025-03230-3